

# Quantitative X-ray microanalysis of thin specimens in the transmission electron microscope; a review

G. W. LORIMER

University of Manchester/UMIST, Department of Metallurgy and Materials Science, Grosvenor Street, Manchester M1 7HS

## Abstract

In a thin specimen X-ray absorption and fluorescence can, to a first approximation, be ignored and the observed X-ray intensity ratios,  $I_A/I_B$ , can be converted into weight fraction ratios,  $C_A/C_B$ , by multiplying by a constant  $k_{AB}$ :

$$C_A/C_B = k_{AB} I_A/I_B.$$

$k_{AB}$  values can be calculated or determined experimentally. The major correction which may have to be made to the calculated weight fraction ratio is for X-ray absorption within the specimen. The activated volume for analysis in a thin specimen is approximately  $100\,000 \times$  less than in a bulk sample. Beam spreading within the specimen can be estimated using a simple formula based on a single elastic scattering event at the centre of the specimen. Examples are given of the application of the technique to obtain both qualitative and quantitative analyses from thin mineral specimens. The minimum detectable mass and the minimum mass fraction which can be measured using the technique are estimated.

KEYWORDS: X-ray microanalysis, transmission electron microscopy, thin specimens.

## Introduction

MODERN analytical electron microscopes provide, in one instrument, morphological information with a resolution of less than  $5 \text{ \AA}$  and crystallographic data and chemical analyses with a spatial resolution of less than  $200 \text{ \AA}$  from a single, thin specimen. The chemical analyses can be obtained by a number of techniques which include X-ray spectrometry, electron energy-loss analysis or Auger-electron spectrometry. At the present time X-ray spectrometry has the distinct advantage over the other techniques in that quantitative analyses can be carried out for all elements for which  $Z > 11$  with a 'conventional' energy-dispersive X-ray (EDX) detector or  $Z \geq 6$  with a 'windowless' or 'ultra-thin window' EDX detector (or  $Z > 3$  with a crystal spectrometer) by simple modifications of procedures used in conventional microprobe analysis of bulk specimens.

Thin film microanalysis is often referred to as STEM microanalysis in the literature, whether the analysis is carried out with an instrument operating in the Scanning Transmission mode or not. In some instruments it is more convenient to operate in the 'conventional' transmission mode, albeit with the

assistance of a strong pre-field of the objective or a 'mini' lens to form a fine probe.

In a thin specimen the spatial resolution for microprobe analysis is dramatically improved compared to a bulk sample. The large, bell-shaped region produced by the diffusion of the electron probe beneath the surface of bulk specimens is absent in a thin foil and, to a first approximation, the activated volume is a cylinder equal to the diameter of the incident electron beam, Fig. 1. This

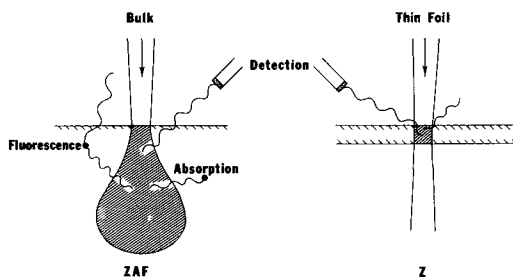


FIG. 1. Schematic representation of the interaction of a high-energy electron beam with a bulk and a thin specimen and the associated X-ray phenomena.

increase in spatial resolution in moving from a bulk to a thin specimen is, typically, a factor of 100 000.

An early example of the use of thin foil specimens to increase the spatial resolution for a qualitative electron probe microanalysis is the work of Lorimer and Champness (1973) on an orthopyroxene from the Stillwater complex, Montana. Transmission electron microscopy of a thin sample showed large (100) augite lamellae; fine, coherent precipitates (Guinier–Preston zones) between the lamellae and a PFZ (precipitate-free zone) immediately adjacent to the lamellae (Fig. 2). The object of carrying out the thin foil electron probe microanalysis was to determine the origin of the PFZ. Fig. 3 shows the results of analyses to determine the ratio of Ca-K $\alpha$ /Si-K X-ray intensities between two augite lamellae. As can be seen from Fig. 3 there is a significant depletion of Ca in the matrix adjacent to the augite lamellae. The PFZ has formed because, in this region, the Ca supersaturation is below that required for nucleation of the coherent G.P. zones.

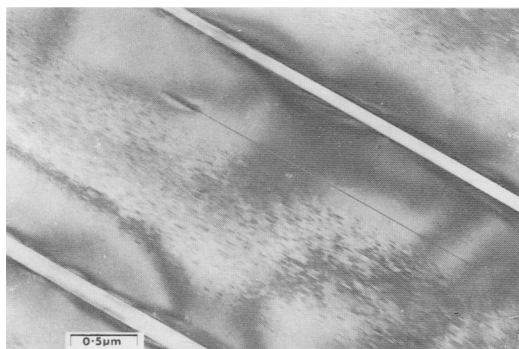


FIG. 2. Electron micrograph of orthopyroxene showing large augite lamellae parallel to (100) matrix, a fine distribution of coherent G.P. zones and a PFZ adjacent to the augite lamellae (Lorimer and Champness, 1973).

#### Quantitative thin foil X-ray microanalysis: the ratio technique

The microprobe analysis of bulk specimens has traditionally been based on a measurement of the absolute X-ray intensity from an unknown and the comparison of this measurement with the absolute X-ray intensity from a suitable standard made under identical instrumental conditions. The appropriate corrections, mainly for stopping power, back-scattering, X-ray absorption and secondary X-ray fluorescence within the specimen, are then applied to the raw data and an iterative procedure, which takes account of the variation in the correc-

tion parameters as a function of specimen composition, is followed to produce a ZAF-corrected analysis.

In a thin specimen the observed X-ray intensity will be a function of specimen thickness as well as composition. Most electropolished or ion-beam thinned specimens for TEM are not parallel-sided, but have an irregular cross-section. It is possible, although difficult and time consuming, to measure the absolute X-ray intensity, monitor the probe current and determine the sample thickness at each analysis point. The measured X-ray intensity can then be compared with the intensity from a bulk or thin specimen standard, suitable corrections made and the composition of the sample determined (see for example Tixier, 1973). In the Life Sciences, where specimens are usually prepared by ultramicrotomy and have a fairly uniform density, absolute X-ray intensity measurements may be determined and related to the weight fraction of individual elements using the background radiation (Hall, 1971) or transmitted electron intensity (Lindens *et al.*, 1982) as a measure of specimen mass thickness. However in the Physical Sciences absolute X-ray intensity measurements are not usually made for thin specimen X-ray microanalysis. Instead a ratio of two or more X-ray intensities is measured and converted into weight fractions. In a sample which is sufficiently thin to carry out quantitative transmission electron microscopy at, say, 100 kV, the incident electrons lose only a small amount of energy in the sample and the ionization cross-

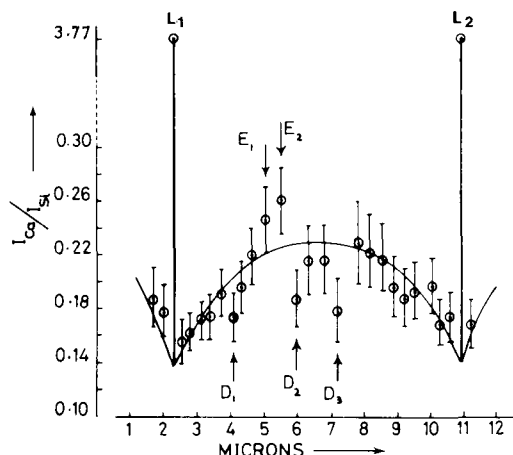


FIG. 3. Variation in Ca concentration,  $I_{Ca}/I_{Si}$ , between two augite lamellae. The positions marked E and D refer to areas enriched or depleted in calcium and correspond to thin lamellae and solute-depleted zones, respectively. L<sub>1</sub> and L<sub>2</sub> are the augite lamellae (Lorimer and Champness, 1973).

section,  $Q$ , the probability of an electron producing an ionization event, is constant along the electron path. To a first approximation X-ray absorption and secondary X-ray fluorescence within the specimen can be ignored. Under these conditions the 'thin film' criterion applies. The absolute X-ray intensity is a function of specimen thickness, as well as composition, but the ratio of two observed X-ray intensities,  $I_A/I_B^*$ , is independent of thickness. This ratio can be simply related to the corresponding weight-fraction ratio,  $C_A/C_B$ , by the equation

$$C_A/C_B = k_{AB} I_A/I_B, \quad (1)$$

where  $k_{AB}$  is a factor which accounts for the relative efficiency of X-ray production and detection. At a given accelerating voltage  $k_{AB}$  is independent of specimen thickness and composition. Equation (1) is the basic formulation of the ratio technique (Cliff and Lorimer, 1975).

A normalisation procedure, e.g.  $\sum C_n = 1$ , must be followed to convert the weight fraction ratios into weight percentages in a sample containing  $n$  detectable elements. If  $I_A \dots I_n$  are measured simultaneously, as can be done with an energy dispersive X-ray detector, the measurements are independent of variations in probe current either during a single analysis or a series of analyses. When the specimen contains elements which are not detected ( $Z < 11$  with a standard energy dispersive detector) assumptions must be made when computing the composition. For example, in mineral specimens oxidation states must be assumed: it is impossible to differentiate between  $Fe_2O_3$  and  $Fe_3O_4$  if ratios are measured and oxygen is not detected.

*Experimentally-determined  $k$  factors.* The first factors were experimentally determined for  $K\alpha$  X-ray lines from a series of silicate mineral standards (Cliff and Lorimer, 1975; Lorimer *et al.*, 1978) and it was convenient to make all of the determinations relative to silicon, i.e.  $k_{XSi}$ . Some of the first experimentally determined  $k_{XSi}$  values are shown in Fig. 4.

McGill and Hubbard (1981) obtained  $k$  factors from a number of silicate minerals, and have given particular attention to the problems of variation in apparent  $k$  value due to elemental loss associated with radiation damage induced by the electron beam. Fig. 5, taken from McGill and Hubbard (1981), shows the variation in the apparent value of  $k_{NaSi}$  as a function of irradiation time for a thin specimen of Amelia albite ( $NaAlSi_3O_8$ ). The data were obtained with an AEI EM6G operating at 100 kV, beam current 200  $\mu A$ , probe diameter 3  $\mu m$ . This current density is well below that available on modern analytical electron microscopes, and high-

\*  $I_A$  and  $I_B$  are X-ray peak integrals with the background  $I_A^B$  and  $I_B^B$  subtracted.

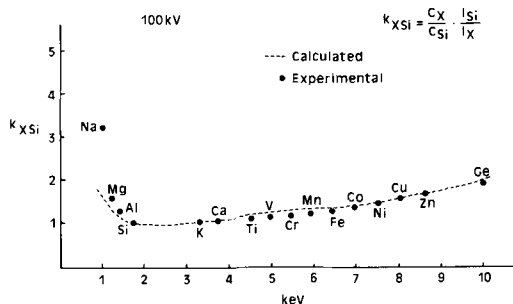


FIG. 4. Experimentally determined  $k_{XSi}$  values from Cliff and Lorimer (1975) and Lorimer *et al.* (1978). The calculated  $k_{XSi}$  data are from Goldstein *et al.* (1977)

lights the care which must be taken when attempting to analyse beam-sensitive materials.

$k$  factors have been measured for both  $K$  and  $L$  lines by Wood *et al.* (1981, 1984) and Schreiber and Wims (1981). Wood *et al.* obtained their data on a Philips EM400T operated at 120 kV while Schreiber and Wims used a JEOL-JEM 200C operated at 100 and 200 kV.

As pointed out above, the original  $k$  factor data were obtained as  $k_{XSi}$  measurements for convenience and it is a simple matter to change from one  $k$  base to another by dividing  $k$  values. There are some advantages in expressing  $k$  values relative to Fe rather than Si. The errors associated with the measurement of Si X-ray intensities, due to Si-K absorption in the specimen, are larger than those associated with Fe-K $\alpha$ . Also, the energy dispersive X-ray detector is almost 100% efficient for the detection of Fe-K $\alpha$  X-rays, while for Si-K X-rays the efficiency is significantly degraded due to absorption in the detector itself. Table 1, from William (1984), summarizes a number of experimentally determined  $k_{XFe}$  values.

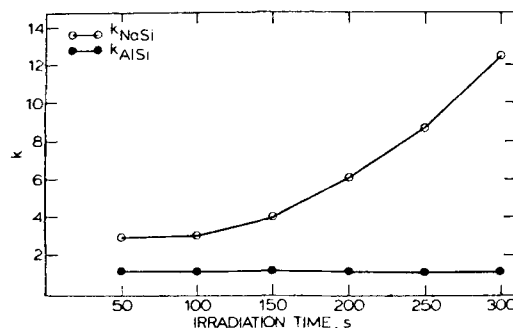


FIG. 5. Variation in  $k_{NaSi}$  and  $k_{AlSi_3}$  with irradiation time for albite feldspar. From McGill and Hubbard (1981).

Table 1. Experimental and Calculated  $k_{XFe}$  Factors for K lines. From Lorimer *et al.* (1977), Wood *et al.* (1981) and Williams (1984).

	Experimental $k_{XFe}$		Calculated $k_{XFe}$ at 120kV
	Lorimer <i>et al.</i> (1977) (100kV)	Wood <i>et al.</i> (1981) (120 kV)	Using ionization cross-sections from Brown (1974)
Na	2.46		1.45
Mg	1.23±.08	.96±0.03	1.03
Al	.92±.08	.86±0.04	0.877
Si	.76±.08	.76±0.004	0.769
P		.77±0.005	0.803
S		.83±0.03	0.817
K	.79	.86±0.014	0.807
Ca	.81±.05	.88±0.005	0.788
Ti	.86±.05	.86±0.03	0.888
Cr	.91±.05	.90±0.006	0.936
Mn	.95±.05	1.04±0.025	0.979
Fe	1.0	1.0	1.0
Co	1.05	.98±0.06	1.066
Ni	1.14±.05	1.07±0.06	1.074
Cu	1.23±.05	1.17±0.03	1.19
Zn	1.24	1.19±0.04	1.255
Nb		2.14±0.06	3.27
Mo	3.38	3.8±0.09	4.91
Ag	6.65	9.52±0.03	

*Calculated k factors.* The physics of X-ray production and detection is fairly well understood, a result of the large amount of effort which has gone into the quantification of bulk microprobe analysis, and  $k$  factors can be calculated from first principles. The characteristic X-ray intensity from an element  $A$ ,  $I_A^*$ , generated by a high-energy electron beam in a thin specimen of thickness  $t$  is given by

$$I_A^* = C_A \omega_A Q_A a_A t / A_A \quad (2)$$

where  $C_A$  is the weight fraction of element  $A$ ,  $\omega_A$  the fluorescence yield,  $Q_A$  the ionization cross-section,  $a_A$  the fraction of the total  $K$ ,  $L$  or  $M$  line which is measured (equal to  $K\alpha/(K\alpha + K\beta)$  for  $K\alpha$  X-rays) and  $A_A$  the atomic weight. In an EDS detector the generated X-ray intensity  $I_A^*$  is attenuated by the Be window, the Au contact layer on the detector surface and the Si dead layer of the detector itself. Thus the detected X-ray intensity,  $I_A$ , is equal to

$$I_A = I_A^* \varepsilon_A \quad (3)$$

where

$$\varepsilon_A = \exp[-(\mu/\rho)_{Be}^A \rho_{Be} X_{Be} - (\mu/\rho)_{Au}^A \rho_{Au} X_{Au} - (\mu/\rho)_{Si}^A \rho_{Si} X_{Si}]$$

and  $(\mu/\rho)$ ,  $\rho$  and  $X$  refer to the mass absorption coefficients, densities and thicknesses of the Be, Au and Si in the detector.

It is necessary to consider a ratio of X-ray production/detection efficiencies, and thus

$$\frac{I_A}{I_B} = \frac{I_A^* \cdot \varepsilon_A}{I_B^* \cdot \varepsilon_B} \quad (4)$$

From equation (1)

$$k_{AB} = \frac{C_A \cdot I_B}{C_B \cdot I_A} \quad (5)$$

and substituting from equation (2) and (3)

$$k_{AB} = \frac{A_A \omega_B Q_B a_B \cdot \varepsilon_B}{A_B \omega_A Q_A a_A \cdot \varepsilon_A} \quad (6)$$

$k_{AB}$  values can be calculated if the relevant terms in equation (6) are known. The fluorescence yield  $\omega$  for the  $K$ ,  $L$  and  $M$  lines can be determined using the equation due to Burhop (1955),

$$(\omega/(1-\omega))^{1/2} = A + BZ + CZ^3 \quad (7)$$

where  $A$ ,  $B$  and  $C$  are constants for a given X-ray line. The ' $a$ ' factor in equation (6) is the fraction of the total X-ray emission from a given shell. Schreiber and Wims (1981) have made measurements of the ' $a$ ' factor for  $K$ ,  $L$  and  $M$  lines.

The detector efficiency term,  $\varepsilon$ , in equation (6) can be calculated, using appropriate  $(\mu/\rho)$  values for  $A$  and  $B$  in Be, Si and Au. The manufacturer should be able to provide information concerning thickness of the Be window (usually about 7.6  $\mu\text{m}$  (0.3 mil)),

the Au contract layer (typically 0.02  $\mu\text{m}$ ) and the Si dead layer (about 0.1  $\mu\text{m}$ ). The  $k$  values for low  $Z$  elements (low energy X-rays) are most strongly affected by the detector parameters.

In Fig. 4 and Table 1 a comparison is made of some experimental and calculated  $k_{\text{XSi}}$  and  $k_{\text{XFe}}$  data. The agreement between the experimentally determined and calculated  $k$  values for  $K$  radiations for  $14 \leq Z \leq 30$  is usually within  $\pm 5\%$  relative. If this quality of analytical data is sufficient (the relative error in an experimentally determined weight fraction ratio will always be larger than that in the relevant  $k$  value), then calculated  $k$  values can be used. If a higher accuracy is required published experimentally-determined  $k$  values are available. For X-rays with an energy of less than 2 keV X-ray detector efficiencies may vary significantly from instrument to instrument and  $k$  values should be determined on the instrument which is to be used to carry out the analyses.

#### X-ray absorption in a thin specimen

The correction which must be applied most frequently to the analysis data generated from thin specimens is for X-ray absorption within the sample. X-ray absorption follows Beer's Law:

$$I_A = I_{oA} e^{-(\mu/\rho)_{\text{SPEC}}^A \rho x} \quad (8)$$

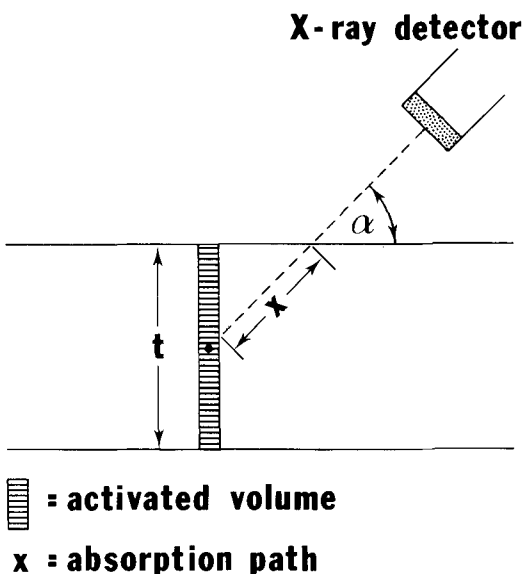


FIG. 6. Geometry used to calculate absorption within the specimen for a normal incident beam.  $x$  is the absorption path (Lorimer, 1983).

where  $I_A$  is the transmitted X-ray intensity,  $I_{oA}$  the initial X-ray intensity and  $(\mu/\rho)_{\text{SPEC}}^A$  is the mass absorption coefficient for element  $A$  in a material with absorption path  $x$  and density  $\rho$ . When the ratio of characteristic X-ray intensities is considered, the difference in X-ray absorption coefficients is the important parameter (if two characteristic X-rays have similar values of  $\mu$  they will be absorbed equally and their intensity ratio will be unaffected). The absorption path length,  $x$ , is shown in Fig. 6, for a specimen normal to the incident beam. If  $t$  is the sample thickness and  $\alpha$  is the angle between the line of the detector and the sample surface, the X-ray intensity ratio  $I_A/I_B$  recorded by the detector will be modified by absorption in the specimen from the ratio recorded for an infinitely thin specimen,  $I_{oA}/I_{oB}$  (no absorption), as given in equation (9).

$$\frac{I_A}{I_B} = \frac{I_{oA}}{I_{oB}} \frac{\left[ \frac{[\mu/\rho]_{\text{SPEC}}^B}{[\mu/\rho]_{\text{SPEC}}^A} \right]}{\left[ \frac{1 - \exp - \{ [\mu/\rho]_{\text{SPEC}}^A \rho t \text{ cosec} \alpha \}}{1 - \exp - \{ [\mu/\rho]_{\text{SPEC}}^B \rho t \text{ cosec} \alpha \}} \right]} \quad (9)$$

The effects of absorption can be included in equation (1) by replacing the  $k_{AB}$  by an 'absorption corrected',  $k_{AB}^*$ ,

$$k_{AB}^* = k_{AB} \underbrace{\left[ \frac{[\mu/\rho]_{\text{SPEC}}^A}{[\mu/\rho]_{\text{SPEC}}^B} \right]}_{\text{Absorption Correction Factor} \equiv \text{ACF}} \left[ \frac{1 - \exp - \{ [\mu/\rho]_{\text{SPEC}}^B \rho t \text{ cosec} \alpha \}}{1 - \exp - \{ [\mu/\rho]_{\text{SPEC}}^A \rho t \text{ cosec} \alpha \}} \right] \quad (10)$$

Note that the absorption path is  $t \text{ cosec} \alpha$  only if the thin foil is normal to the incident beam.

The effects of absorption in the specimen on the observed X-ray intensity ratios have been calculated for pure orthopyroxene,  $\text{MgFeSi}_2\text{O}_6$ , as a function of thickness. These results are shown in Fig. 7. They clearly show that while the observed Fe/Si X-ray intensity ratio increases as a function of thickness because the Si-K radiation is preferentially absorbed, the observed Mg/Si X-ray intensity ratio decreases, due to the preferential absorption of Mg-K radiation, relative to Si-K radiation. Whether or not it is necessary to make an absorption correction depends on the sample thickness, the difference in the  $(\mu/\rho)$  values in the specimen of the elements of interest and the accuracy required. If the estimated error due to absorption is significantly less than that due to the limitations to accuracy imposed by counting statistics it is not necessary to make an absorption correction. This is often the case with silicates of thicknesses up to 0.2  $\mu\text{m}$ .

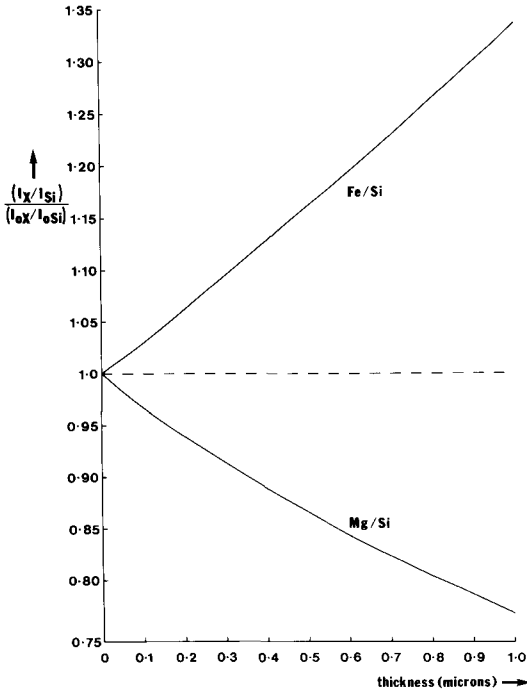


FIG. 7. Calculated variation in observed Fe-K/Si-K and Mg-K/Si-K X-ray intensity ratios as a function of thickness relative to the ratios observed for an infinitely thin specimen (Champness *et al.*, 1982).

### Quantitative analysis of fine intergrowths in mica

Quantitative analytical electron microscopy has been used to analyse the phases in a paragonite mica which contained a fine intergrowth of margarite and muscovite lamellae\*, fig. 8. The same (bulk) specimen had been previously analysed using conventional electron probe microanalysis, and the results obtained are plotted on the margarite, muscovite, paragonite ternary, Fig. 9. The bulk microprobe results, filled squares, are scattered over the ternary diagram. Analyses by analytical electron microscopy, which were quantified using experimental  $k$  values, are plotted as open triangles in Fig. 9. Corrections were made for absorption using an estimated sample thickness of, typically, 100 nm. These data are concentrated at three points, which clearly show that three phases, of fixed composition, are present in the specimen.

The ability to analyse, quantitatively, mineral intergrowths on the scale described above is of particular importance in determining phase rela-

\* The author is indebted to Dr Anne Feenstra for permission to quote these unpublished results.

tionships in metamorphic rocks, e.g. Brearley, 1987. The technique also has great potential in experimental petrology.

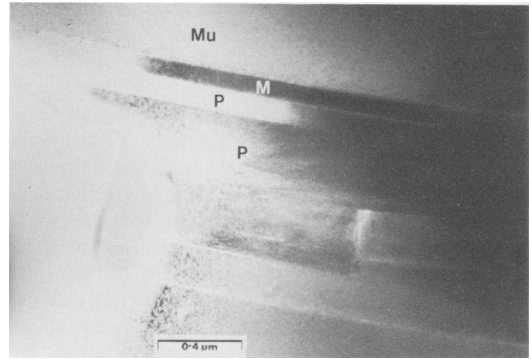


FIG. 8. Transmission electron micrograph showing fine intergrowths of margarite (M) and muscovite (Mu) lamellae in a matrix of paragonite (P) (Feenstra and Champness, unpubl.).

### X-ray fluorescence in thin specimens

The characteristic X-ray intensity emitted by an element  $A$  may be enhanced by secondary X-ray fluorescence from the characteristic X-rays emitted by a second element  $B$ . This leads to an apparent increase in the concentration of  $A$ . Secondary X-ray fluorescence can only occur if the energy of the  $B$  X-rays is greater than the excitation energy,  $E_c$ , of  $A$ .

Fluorescence effects in thin specimens are less than those in bulk specimens due to the smaller volume of material available to be fluoresced and it is only necessary to make a correction to data from thin specimens when strong characteristic X-ray fluorescence is predicted in the equivalent bulk specimen.

Nockolds *et al.* (1979) considered that primary X-ray generation occurs uniformly along the line of the electron beam, Fig. 10, and they predict that the fluorescence enhancement is given by

$$\frac{I_A^F}{I_A} = C_B \omega_B \left( \frac{r_A^{-1}}{r_A} \right) \frac{A_A}{A_B} \left[ \frac{\mu}{\rho} \right]_A^B \cdot \frac{U_B \ln U_B}{U_A \ln U_A} \cdot \frac{\rho t}{2} \left[ 0.923 - \ln \left[ \frac{\mu}{\rho} \right]_{\text{SPEC}}^B \right] \sec \alpha \quad (11)$$

where  $I_A^F/I_A$  is the ratio of fluorescence intensity to primary intensity,  $\omega_B$  is the fluorescence yield of element  $B$ ,  $r_A$  is the absorption edge jump ratio of element  $A$ ,  $[\mu/\rho]_A^B$  and  $[\mu/\rho]_{\text{SPEC}}^B$  are the mass absorption coefficients of element  $B$  radiation in

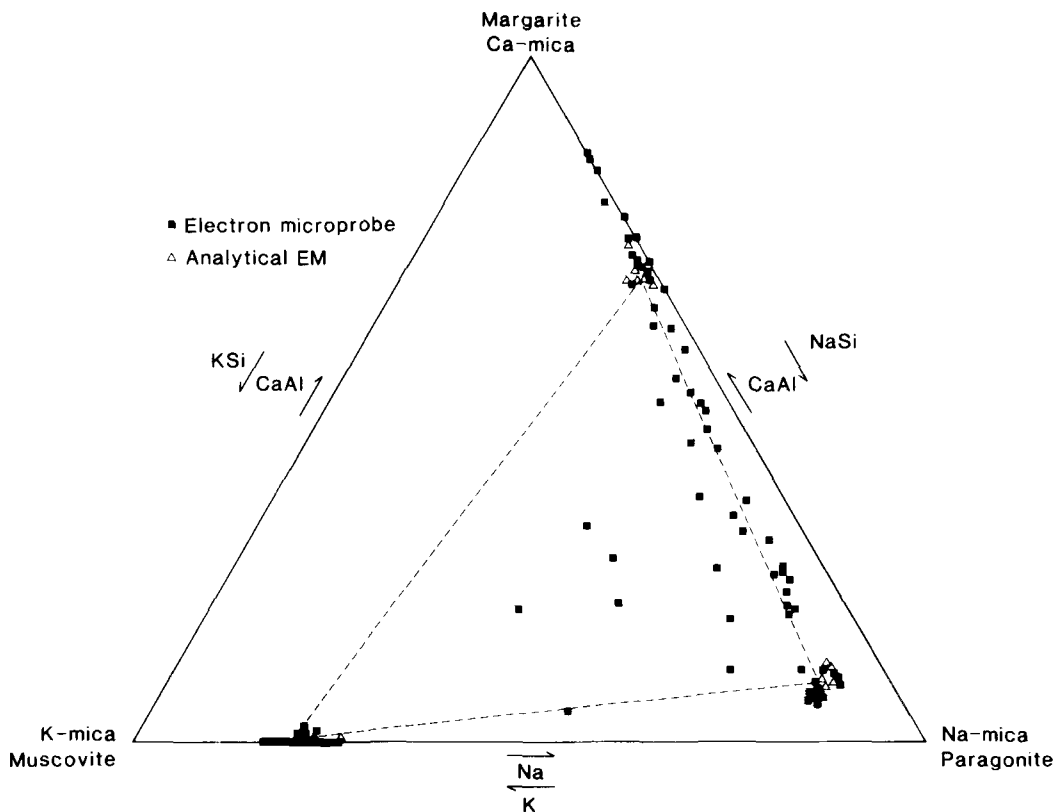


FIG. 9. Muscovite, margarite, paragonite ternary section showing bulk microprobe ■ and analytical electron microscopy ▲ analyses (Feenstra and Champness, unpubl.).

element  $A$  and the specimen respectively,  $A_A$  and  $A_B$  are atomic weights and  $U_A$  and  $U_B$  are the over voltages for the characteristic radiation of  $A$  and  $B$  and  $\alpha$  is the angle of tilt.

For a binary alloy  $AB$  where  $B$  is fluorescing  $A$ , the corrected composition is given by

$$C_A/C_B = k_{AB} \frac{I_A}{I_B} \cdot \frac{1}{\left[1 + \frac{I_A^F}{I_A}\right]} \quad (12)$$

When both absorption and characteristic fluorescence corrections are necessary

$$C_A/C_B = k_{AB} \frac{I_A}{I_B} \cdot [ACF] \cdot \frac{1}{\left[1 + \frac{I_A^F}{I_A}\right]} \quad (13)$$

The effects of absorption are almost always much more serious than characteristic fluorescence for specimens of similar thicknesses. Fluorescence enhancement due to the continuum is much less than that due to characteristic fluorescence and can be safely ignored in thin specimens.

### Beam broadening in the specimen

The spatial resolution for analysis of a thin specimen is limited by the initial probe diameter and the amount of beam broadening,  $b$ , which

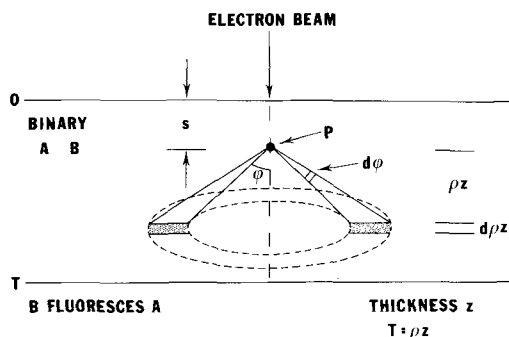


FIG. 10. Geometry used by Nockolds *et al.* (1979) to calculate fluorescence enhancement in a thin specimen.

occurs between the top and bottom of the foil. The first model of beam broadening in a thin foil was developed by Reed in the paper by Goldstein *et al.* (1977). Reed assumed that a single, Rutherford-scattering event occurred at the centre of the foil, Fig. 11, and he defined the X-ray source size as that volume in which 90% of the electron trajectories lay. The beam broadening,  $b$ , from a point analysis probe was given by

$$b = 6.25 \times 10^5 \frac{Z}{E_0} \left[ \frac{\rho}{A} \right]^{1/2} t^{3/2} \text{ cm} \quad (14)$$

where  $\rho$  is in  $\text{g cm}^{-3}$ ,  $E_0$  in eV and  $t$  in cm.

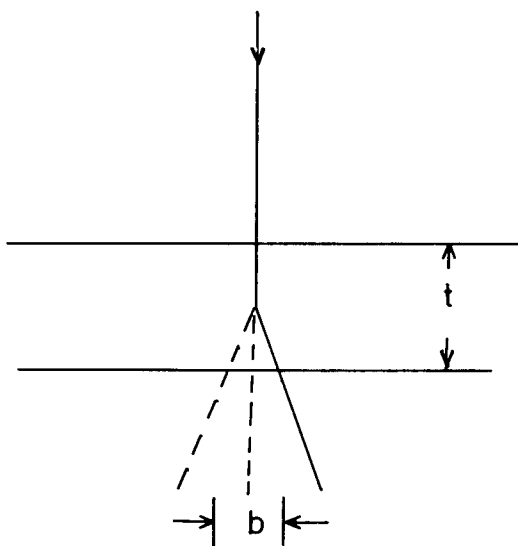


FIG. 11. Simple model for beam broadening,  $b$ , from Goldstein *et al.* (1977).

Monte Carlo techniques have been used by a number of authors, including Newbury and Myklebust (1979) and Kyser (1979) to model the electron intensity distribution in thin foils, e.g. Fig. 12. The predictions of beam broadening using the simple model of Reed agree well with Monte Carlo calculations up to thicknesses of a few mean free paths.

The difficulty in attempting to determine solute segregation or solute distributions using either an analytical or Monte Carlo approach is that the solute distribution, the electron distribution in the incident probe and the electron distribution within the specimen are all unknown. If the incident electron distribution is assumed to be Gaussian

with a known FWHM and the electron distribution in the specimen is known, it is, in theory, possible to deconvolute the observed variation of solute concentration as a function of distance to determine the true distribution. However, if the solute distributions occur over distances equal to or less than the FWHM of the incident electron probe this deconvolution is often in practice impossible to carry out.

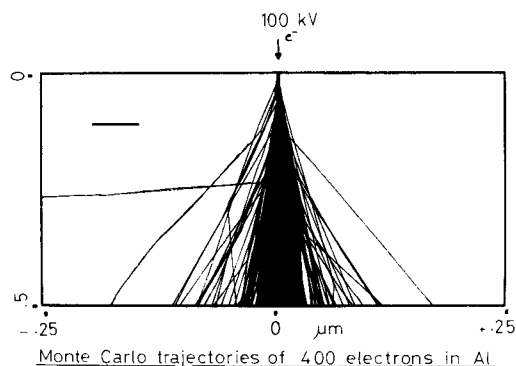


FIG. 12. Monte Carlo calculations of electron trajectories in Al 500 nm thick. From Cliff and Lorimer (1981).

Experimental measurements of beam broadening have been made by a numbers of workers. Champness *et al.* (1982) measured broadening across augite lamellae in an orthopyroxene and a similar geometry was used by Romig and Goldstein (1979) to measure broadening in a Fe-Ni alloy. Vander Sande and Hall (1979) and Doig and Flewitt (1977) attempted to measure beam broadening by monitoring solute segregation at grain boundaries. Hutchings *et al.* (1979) and Stephenson *et al.* (1981) have measured beam broadening with thin samples of silicon which have strips of either gold or chromium evaporated onto one surface. Analyses were made across the silicon/metal interface first with the strips on the top of the specimen and then with them on the bottom. The difference between the two results was equal to the beam broadening in the specimen.

In most of the experiments carried out to measure beam broadening, the extent of broadening has been found to be similar to the incident beam diameter (this is particularly true at specimen thicknesses suitable for quantitative electron microscopy, i.e. the thickness of real interest). Thus the quality of the data is modest and it has not been possible to differentiate between the predictions of the various theoretical models.

**Thickness measurements**

Determination of the beam broadening and the corrections for X-ray absorption and fluorescence within the specimen require the knowledge of the sample thickness.

*Parallax measurements.* If a planar feature, e.g. a slip trace, precipitate or stacking fault, whose crystallography is known, cuts the top and bottom surfaces of the foil its projected width,  $W$ , can be measured and the thickness,  $t$ , calculated as  $t = W/M \tan\theta$  where  $\theta$  is the angle between the feature and the foil surface and  $M$  is the magnification.

*Contamination spots.* When a probe a few nanometers in diameter is focussed on the specimen a contamination spot will be formed on the top and bottom surfaces of the foil under all but the most stringent conditions of specimen cleanliness and microscope vacuum. If the foil is then tilted through an angle  $\theta$  the separation of the contamination spots  $X$  can be used to calculate the thickness using the relationship  $t = X/M \sin\theta$ . The technique has the advantage of being rapid and easy to use, but it can seriously overestimate sample thickness. Rae *et al.* (1981) have shown that the fine contamination spots often sit on top of an almost invisible 'foothill' of contamination and thus the thickness plus the background contamination are measured.

*Convergent beam diffraction.* The most accurate technique for the measurement of the thickness of crystalline specimens is convergent-beam diffraction. Under two-beam diffraction conditions Kossel-Möllenstedt fringes are observed in the transmitted and diffracted disks, the spacing of which can be used to measure the specimen thickness (see Champness, 1987).

This technique was first described in detail by Kelly *et al.* (1975). The application and limitations of the technique have been discussed by Allen (1981). With care the technique can give thickness measurements with an accuracy of  $\pm 5\%$  in metallic systems.

However, the technique probably has a very limited application to most mineral specimens. The large lattice parameters of minerals, and hence their small reciprocal lattice dimensions, mean that it will be difficult to obtain diffraction disks which contain sufficient fringes (at least 3). Also because of the short reciprocal lattice distances it is difficult to obtain true 'two-beam' kinematic conditions, and hence the fringe spacing will be difficult to interpret.

**Accuracy of analysis**

The fundamental limit of accuracy of the weight fraction ratio obtained using the ratio techniques arises from the X-ray counting statistics. X-ray counting statistics obey Gaussian behaviour for which the standard deviation  $\sigma$  is equal to  $\sqrt{N}$ , the square root of the number of counts accumulated. For a Gaussian distribution there is a 95% probability that the true value of  $N$  will lie within  $2\sigma$  of the mean,  $N$ , and the percentage error in the number of counts is  $2\sqrt{N}/N \times 100$ . In equation (1) the total percentage error in  $C_A/C_B$  for a single measurement is equal to the square root of the sum of the squares of the percentage errors in  $I_A$ ,  $I_B$  and  $k_{AB}$ . The quality of the analysis which can be obtained for a binary alloy purely due to counting statistics for various values of  $N_A$  and  $N_B$  is given in Table 2. It is assumed that the percentage error in the  $k_{AB}$  value is constant at  $\pm 2\%$ .

If  $n$  measurements are made of the 'same' composition then the total relative error in  $I_A/I_B$  at the 95% confidence level is given by Romig and Goldstein (1980).

$$\frac{1}{\sqrt{n}} \frac{t_{95}^{n-1} \sigma}{(I_A/I_B)} \times 100 \tag{15}$$

where  $t_{95}^{n-1}$  is the student  $t$  value and  $\sigma$  is the standard deviation, calculated for  $n$  values of the

Table 2. The effect of counting statistics on the quality of the analysis for a binary alloy. The error in  $k_{AB}$  is assumed to be constant at  $\pm 2\%$ .

$N_A$ (counts)	$\sigma N_A$	percentage error in $N_A$ at $\pm 2\sigma$	$N_B$ (counts)	$\sigma N_B$	percentage error in $N_B$ at $\pm 2\sigma$	total percentage error in $C_A/C_B$ at $\pm 2\sigma$
1,000	32	6.4	1,000	32	6.4	$\pm 9.3\%$
10,000	100	2.0	1,000	32	6.4	$\pm 7.0\%$
10,000	100	2.0	10,000	100	2.0	$\pm 3.5\%$
100,000	320	0.6	100,000	320	0.6	$\pm 2.1\%$

ratio  $I_A/I_B$ ,  $\overline{(I_A/I_B)}$  is the average value of  $I_A/I_B$  and

$$\sigma = \sqrt{\frac{\sum_{i=1}^n (I_A/I_B)_i - \overline{(I_A/I_B)}^2}{n-1}}$$

### Minimum detectable limit or minimum mass fraction (MMF)

The minimum detectable limit corresponds to the detection of the smallest significant X-ray signal above background. A peak containing  $I_B$  counts is assumed to be real if it is larger than three standard deviations of the background, i.e.

$$I_B \geq 3 \sqrt{I_B^b} \quad (16)$$

where  $I_B^b$  is the background intensity for element B. In a binary system AB equation (1) can be used to convert the number of X-ray counts into weight percent.

$$\frac{I_A}{I_B} = k_{AB} \frac{C_A}{\text{MMF}_B} \quad (17)$$

$$\text{MMF}_B = k_{AB}^{-1} \frac{C_A \cdot 3}{I_A} \sqrt{I_B^b} \quad (18)$$

Experience has shown that without taking any special precautions to reduce the level of the background signal MMF values of between 0.5 and 1 wt. % can be obtained.

### Minimum detectable mass (MDM)

The MDM that can be measured is given, using the equations developed by Joy and Maher (1979), as

$$\text{MDM} = \frac{1}{I_A^+ \cdot \tau \cdot J} \quad (19)$$

where  $\tau$  is the counting time,  $J$  is the electron current density and  $I_A^+ = Q_A \omega_A a_A \varepsilon_A$ , where  $\varepsilon_A$  is the EDS detector efficiency.

To improve the MDM only  $\tau$  and  $J$  can be increased as  $I_A^+$  is constant for a given element and detector. With a thermionic gun, values of MDM are in the region of  $10^{-19}$  to  $10^{-20}$  g.

### Enhanced X-ray emission

In the vicinity of extinction contours, where the incident electron beam is interacting strongly with the specimen, enhanced X-ray emission is observed (Cherns *et al.*, 1973). If the sample is a random solid solution, X-ray emission from all elements is increased and the observed X-ray ratio is not affected (Lorimer *et al.*, 1978). However in ordered solid solutions significant variations in the ratio of X-ray intensities have been observed. The effect has been used to advantage in the development

of ALCHEMI, Atom Location by Channelling Enhanced Microanalysis (Spence and Taftø, 1983).

The thin, single crystal is orientated so that the specific atom sites are parallel to the incident electron beam, and that parallel and not convergent illumination is used. If the species of interest is preferentially located on these atom sites enhanced X-ray emission will be observed. The technique has been used by Taftø (1982) to determine the site occupancies of Cr, Al, Fe and Mg in chromite spinels and by Taftø and Spence (1982) to determine site occupancies of Fe and trace elements in an Mg-Fe olivine. Taftø and Buseck (1983) determined the Al content of the T1 site in an orthoclase feldspar and obtained results in good agreement with X-ray diffraction.

If the investigator wishes to minimise the effects of channelling enhanced emission, analyses should be carried out with the specimen orientated well away from the exact Bragg condition and with a highly convergent, rather than a parallel, incident electron beam.

### X-ray microanalysis of second phase particles in thin foils

A problem of particular interest to the analytical electron microscopist is the *in-situ* microanalysis of second phase particles in thin foils (Cliff *et al.*, 1984). The X-ray intensity  $I_A$ , from an element A is proportional to the weight fraction of that element,  $C_A$ , and the total X-ray intensity  $I_A^T$  from a thin sample which contains second phase particles is given by

$$I_A^T \propto C_A^M L_M + C_A^P L_P,$$

where  $C_A^M$  and  $C_A^P$  are the weight fraction of element A in the matrix and particle, respectively, and  $L_M$  and  $L_P$  the respective electron path lengths. The electron path length may be 100% in the matrix, Fig. 13a, 100% in the particle, Fig. 13b, or partially in both, Fig. 13c. If element A, a solvent, is

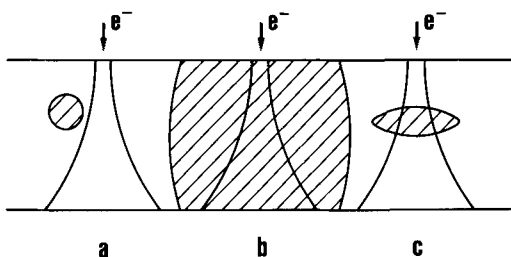


FIG. 13. Schematic diagram of possible electron paths in a thin sample containing second phase particles (shown hatched). (Lorimer *et al.*, 1984).

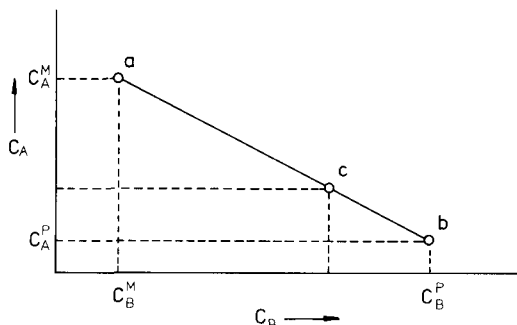


FIG. 14. Schematic diagram of the analytical data obtained from the sample shown in Fig. 13 (Lorimer *et al.*, 1984).

concentrated in the matrix and *B*, a solute, is concentrated in the precipitate, then the analysis of *A* from the regions shown in Fig. 13 can be expressed against *B*, graphically, as in Fig. 14, where  $C_B^M$  and  $C_B^P$  are the weight fractions of element *B* in the matrix and particle, respectively. If both the particle and matrix have fixed compositions the data will plot on a straight line. The effect of changing the proportion of the electron beam path which is in the particle is to move point (c) along the line. It may be difficult to obtain the point (b), due to the small size of the second phase particles and their preferential attack during specimen preparation. However, if the particle and the matrix have fixed compositions, the data will extrapolate through the true, second-phase composition.

*Second-phase particles in sphalerite* (Lorimer *et al.*, 1984). In a study of textural relationships in sulphides, sphalerite (ZnS) from a lead-zinc vein at Tyndrum, Scotland, showed evidence of partial replacement by chalcopyrite,  $\text{CuFeS}_2$ . Apparently homogeneous areas of this sphalerite were found by bulk microprobe analysis to contain between 1.0 and 0.2 wt. % Cu and approximately 0.5 wt. % Fe.

Examination of ion-beam thinned specimens in the TEM revealed the presence of both particles and 'dendrites'. The analytical data from the particles, Fig. 15a, extrapolates to pyrite,  $\text{FeS}_2$ . The identification of the particles as pyrite was confirmed by electron diffraction. Analytical data from the dendritic-shaped particles, Fig. 15b, extrapolate to high chalcocite,  $\text{Cu}_2\text{S}$ , containing a small amount of iron.

The pyrite and the high chalcocite appear to have formed from the late-stage hydrothermal fluids that precipitated the chalcopyrite. This provides evidence for the formation of an intermediate phase during the replacement of sphalerite by chalcopyrite.

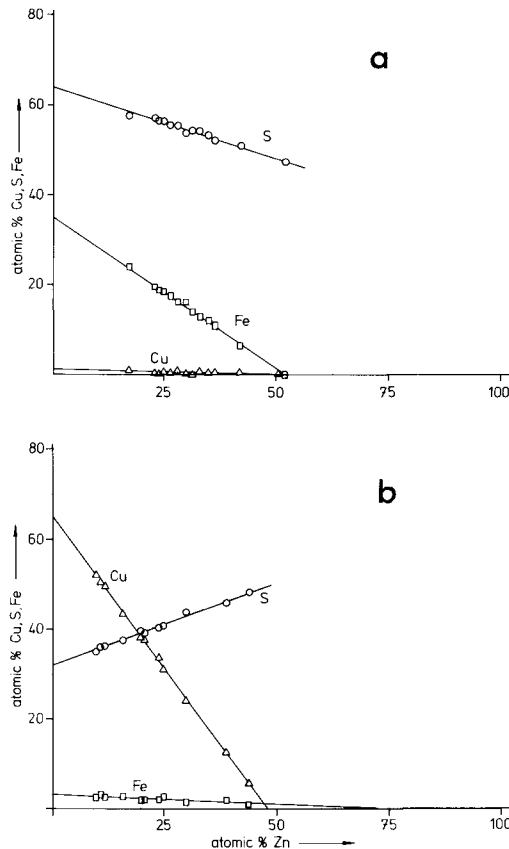


FIG. 15. (a) Analysis of second-phase particles of  $\text{FeS}_2$  in sphalerite (Lorimer *et al.*, 1984). (b) Analysis data from dendritic-shaped particles of  $\text{Cu}_2\text{S}$  in sphalerite (Lorimer *et al.*, 1984).

### Summary and conclusions

The microprobe analysis of thin specimens, based on the ratio technique and with experimentally determined or calculated  $k_{AB}$  factors, is an effective method of obtaining quantitative chemical information with a spatial resolution of a few tens of nanometers. The correction which must be most frequently applied to data obtained using the technique is that for X-ray absorption within the specimen. Secondary X-ray fluorescence in thin specimens is much less than in the bulk samples and corrections need be applied only when very strong secondary fluorescence is predicted in an equivalent bulk specimen.

### References

- Allen, S. M. (1981) *Phil. Mag.* **A43**, 325.  
Brearley, A. J. (1987) *Mineral. Mag.* **51**, 93-106.

- Brown, D. B. (1974) In *Handbook of Spectroscopy*, 1 (J. W. Robinson, ed.) CRC Press, Cleveland, 248.
- Burhop, E. H. S. (1955) *J. Phys. Radium*, **16**, 625.
- Champness, P. E. (1987) *Mineral. Mag.* **51**, 33-48.
- Cliff, G. and Lorimer, G. W. (1982) *Ultramicrosc.* **8**, 121.
- Cherns, D., Howie, A., and Jacobs, M. H. (1973) *Z. Naturf.* **28a**, 171.
- Cliff, G. and Lorimer, G. W. (1975) *J. Microsc.* **103**, 203.
- (1981) In *Quantitative Electron Microscopy with High Spatial Resolution* (G. W. Lorimer, M. H. Jacobs and P. Doig, eds.) The Metals Society, 47.
- Powell, D. J., Pilkington, R., Champness, P. E., and Lorimer, G. W. (1984) In *Electron Microscopy and Analysis, 1983* (P. Doig, ed.) I.O.P., London, 63.
- Doig, P. and Flewitt, P. E. J. (1977) *J. Microsc.* **110**, 107.
- Goldstein, J. I., Costley, J. L., Lorimer, G. W., and Reed, S. J. B. (1977) *SEM 1977* (O. Johari, ed.) Pub. IIRTI, Chicago, 315.
- Hall, T. A. (1971) In *Physical Techniques in Biological Research*, 1A, 2nd Ed., Academic Press, London, 157.
- Hutchings, R., Loretto, M. H., Jones, I. P., and Smallman, R. E. (1979) *Ultramicrosc.* **3**, 401.
- Joy, D. C. and Maher, D. M. (1979) *SEM 1979* (O. Johari, ed.) IIRTI, Chicago, 325.
- Kelly, P. M., Jostens, A., Blake, R. G., and Napier, J. G. (1975) *Phys. Stat. Sol.* **31**, 771.
- Kyser, D. F. (1979) In *Introduction to Analytical Electron Microscopy* (J. Hren, J. I. Goldstein and D. C. Joy, eds.) Plenum Press, New York, 199.
- Lindens, P. W. J., Zahniser, D. J., Stols, A. L. H., and Stadhoudens, A. M. (1982) *J. Histochem. Cytochem.* **30**, 637.
- Lorimer, G. W. (1983) In *Quantitative Electron Microscopy* (J. N. Chapman and A. J. Craven, eds.) Proc. 25th Scottish Universities Summer School in Physics, Glasgow, August 1983.
- and Champness, P. E. (1973) *Am. Mineral.* **58**, 243.
- Al-Salman, S. A., and Cliff, G. (1978) In *Electron Microscopy and Analysis 1977* (D. C. Misell, ed.) I.O.P., London, 369.
- Cliff, G., Champness, P. E., Dickinson, C., Hasan, F., and Kenway, P. (1984) In *Analytical Electron Microscopy 1984* (D. B. Williams and D. C. Joy, eds.) San Francisco Press, San Francisco, 153.
- McGill, R. J. and Hubbard, F. H. (1981) In *Quantitative Microanalysis with High Spatial Resolution* (G. W. Lorimer, M. N. Jacobs and P. Doig, eds.) The Metals Society, London, 30.
- Newbury, D. F. and Myklebust (1979) In *Microbeam Analysis 1979* (D. B. Wittry, ed.) San Francisco Press, San Francisco, 173.
- Nockolds, C., Nasir, M. J. and Lorimer, G. W. (1979) In *Electron Microscopy and Analysis* (T. Mulvey, ed.) I.O.P., London, 417.
- Rae, D. A., Scott, V. D. and Love, G. (1981) In *Quantitative Microanalysis with High Spatial Resolution* (G. W. Lorimer, M. H. Jacobs and P. Doig, eds.) The Metals Society, 57.
- Romig, A. D. and Goldstein, J. I. (1979) *Microbeam Analysis 1979* (D. E. Newbury, ed.) San Francisco Press, San Francisco, 124.
- (1980) *Met. Trans.* **11A**, 1151.
- Schreiber, T. P. and Wims, A. M. (1981) In *Microbeam Analysis, 1981* (R. Geiss, ed.) San Francisco Press, San Francisco, 317.
- Spence, J. C. H. and Taftø, H. (1983) *J. Microsc.* **130**, 147.
- Stephenson, T. A., Loretto, M. H. and Jones, I. P. (1981) In *Quantitative Microanalysis with High Spatial Resolution* (G. W. Lorimer, M. H. Jacobs and P. Doig, eds.) Metals Society, London, 53.
- Taftø, J. (1982) *J. Appl. Crystallogr.* **15**, 378.
- and Buseck, P. (1983) *Am. Mineral.* **68**, 944.
- and Spence, J. (1982) *Science*, **218**, 49.
- Tixier, R. (1973) Ph.D. Thesis, University of Paris, Orsay, No. 196.
- Vander Sande, J. B. and Hall, E. L. (1979) In *Electron Microscopy and Analysis 1979* (T. Mulvey, ed.) I.O.P. London, 183.
- Williams, D. B. (1984) *Practical Analytical Electron Microscopy in Materials Science*, Philips Electronic Instruments, Inc., Electron Optics Publishing Group.
- Wood, J. E., Williams, D. E. and Goldstein, J. I. (1981) In *Quantitative Microanalysis with High Spatial Resolution* (G. W. Lorimer, M. H. Jacobs and P. Doig, eds.) The Metals Society, London, 24.
- (1984) *J. Microsc.* **133**, 255.

[Revised manuscript received 1 September 1986]